

# Effect of High-cyclic Loads on Dynamic Response of Reinforced Concrete Slabs

Adiza Jamadin\*, Zainah Ibrahim\*\*, Mohd Zamin Jumaat\*\*\*, and Ezahtul Shahreen Ab Wahab\*\*\*\*

Received May 14, 2018/Revised August 15, 2018/Accepted October 21, 2018/Published Online January 18, 2019

## Abstract

Bridge reinforced concrete deck slabs are often subjected to various cyclic loadings—making regular checks for fatigue damage necessary. Several experiments on reinforced concrete structures were conducted to evaluate its mechanical fatigue behaviour. Nevertheless, adequate experimental investigations on its dynamic properties are still needed. This paper reports on the test performed on three identical reinforced concrete slabs, with different cyclic load number and after the cycles, the load was increased up to the static failure. Modal testing was performed after each step of loading to assess their dynamic performance using modal parameters (natural frequencies, mode shapes and damping ratios). Finite element model was used to predict the natural frequency of the reinforced concrete slabs and their reliability was checked through model updating. The results showed the intensity of fatigued structures causes significant changes to the modal parameters and structural loading capacity. The study explores how fatigued structure can be assessed from dynamic performance, and also can be quantified through its structural stiffness, ultimately offering a better way of using non-destructive modal testing in identifying its structural health as compared to conventional testing techniques.

Keywords: *modal testing, fatigue, reinforced concrete slab, modal parameters, structural stiffness*

## 1. Introduction

Assessment of existing fatigued structures is an important aspect in the entire civil engineering infrastructure. This is critical in most loaded infrastructures i.e. bridges which are continually subjected to dynamic loading, causing the materials to fatigue with time (Benmokrane *et al.*, 2006; Liu *et al.*, 2012; Oh *et al.*, 2005; Suthiwarapirak and Matsumoto, 2006). As these structures are constantly under load, frequent structural monitoring is needed to assess the structural health levels in order to prevent any catastrophic failures, which are not only exorbitant to restore but may also result in casualties. According to Hsu (1981), bridge structure is categorized under high-cycle fatigue load, characterised by the application of large load cycle number at low-stress levels. Due to the population and economic growth, traffic intensity has increased remarkably, and in response, this accelerates the structural fatigue rate which practically leads to internal cracking and deterioration of stiffness and load-carrying capacities of the concrete structure.

Moving loads from vehicles that act on Reinforced Concrete (RC) bridge decks cause the super structure consisting of beams and slabs to deflect from its equilibrium position relatively quick. The mass and inherent elasticity of the structure tend to restore the bridge deck back to its equilibrium position but in the

meantime causing a series of vibrations due to the motion of vehicles on the deck. The mechanical vibration component can be determined via a vibration test, a non-destructive technique that detects micro-cracking due to cyclic load by studying the parameters extracted from the concrete. For this purpose, the use of Non-Destructive Test (NDT) and Non-Destructive Evaluation (NDE) are highly favourable and effective since the existing structures sustain no damages throughout the process with no disruption to normal structure usage (Bayraktar *et al.*, 2010; Ko and Ni, 2003). These methods are also more accurate than conventional visual inspection of the structures, which is highly subjective and does not give a quantifiable structural health. One of the commonly used NDT for measuring structural health is the vibration testing method, which is also known as the modal testing and the modal analysis (Kashif Ur Rehman *et al.*, 2016; Yoon *et al.*, 2009; Kutanis *et al.*, 2017).

It can be seen that considerable research has indeed been done to investigate the dynamic behaviour of concrete structures in various undamaged (Altunişik *et al.*, 2018; Kutanis *et al.*, 2017) and damaged conditions under incremental statically applied load (Carreira *et al.*, 2017; Carvelli *et al.*, 2010; Hsu, 1981; Lenschow, 1980; Liu *et al.*, 2012; Oh *et al.*, 2005; Sivagamasundari and Kumaran, 2008; Kourehli *et al.*, 2013). However, appropriate dynamic behaviour of concrete structures subjected to fatigue

\*Ph.D. Student, Dept. of Civil Engineering, University of Malaya, Kuala Lumpur 50603, Malaysia; Senior Lecturer, Faculty of Civil Engineering, Universiti Teknologi MARA, Shah Alam 40450, Selangor, Malaysia, Shah Alam 40450, Malaysia (Corresponding Author, E-mail: adiza@salam.uitm.edu.my)

\*\*Associate Professor, Dept. of Civil Engineering, University of Malaya, Kuala Lumpur 50603, Malaysia (E-mail: zainah@salam.uitm.edu.my)

\*\*\*Professor, Dept. of Civil Engineering, University of Malaya, Kuala Lumpur 50603, Malaysia (E-mail: zamin@salam.uitm.edu.my)

\*\*\*\*Lecturer, Faculty of Civil Engineering, Universiti Malaysia Pahang, Gambang 26300, Malaysia (Email: ezahtul@ump.edu.my)

loads and fatigue analysis are still lacking in the open literature (Plachy and Polak, 2007; Prasad and Seshu, 2010). This is essential in actual civil engineering applications, in which structures i.e., bridges, roads, airfields, dams, offshore structures, etc. are susceptible to cyclic loading that causes fatigue. Therefore, this research introduce high-cycle fatigue loading onto RC slabs to simulate the effects of fatigue loading as in actual bridge's RC deck. The residual load carrying capacities of fatigued RC slabs are then determined through static test. Modal testing method was applied on all the RC slabs to determine the dynamic characteristics of fatigued RC slabs. More importantly, it was demonstrate the relevance of applying this method in determining the relationship between fatigue cycles and load carrying capacity, which then represents efficient monitoring of structural health in non-destructive techniques.

## 2. Experimental Investigation

Various parameters affect the dynamic response of fatigued RC slabs. This study investigates the effect of cyclic load number variation (1, 1.5 and 2 million) and its corresponding remaining load carrying capacity. The RC slab specimens were divided into two main groups based on different type of testing were performed. A total of three RC slab specimens were tested under fatigue and static loading conditions in four point bending and another three RC slab specimens were performed on the four point static test only for obtaining its ultimate static bending strength. The test matrix is presented in Table 1.

### 2.1 Description of the Tested Specimens

The RC slab specimens were constructed by using ready-mixed concrete through the mix of crushed stone as coarse aggregate, natural river sand as fine aggregate, cement and water. Normal weight concrete with characteristics compressive strength of 40 MPa was obtained from the cube compressive strength test at 28 days according to BS 1881 (1983). Ribbed steel bars, 10 mm in diameter, were embedded for internal longitudinal reinforcement in the slabs. The steel bars had yield strength of 500 MPa according to the manufacturer's certificate. For a validation, a tensile test was conducted to determine tensile strength for the steel. The test was conducted according to BS 4449 (2005) by using a Universal Testing Machine (UTM). The result of the testing shows the steel had average nominal yield strength of 550 MPa. The geometry of the RC slabs were 2.2 m long with effective spans of 2 m and rectangular cross-sections with a

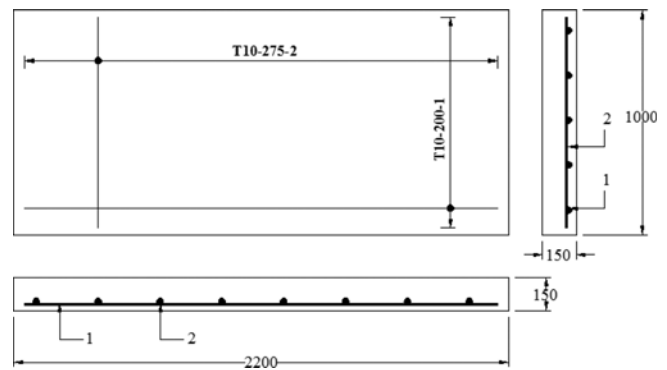


Fig. 1. RC Slab Specimen Details (unit in mm)

dimension of 1,000 × 150 mm. Fig. 1 illustrates the details of the RC slab. The Young's modulus of concrete,  $E_c$  was calculated using the empirical expression shown at Eq. (1) (Nawy, 2005), where  $f_c$  is the 28 day cube strength, as follows:

$$E_c = 4730 \sqrt{f_c} \quad (1)$$

### 2.2 Static and Fatigue Test

The test setup of static and fatigue test are shown in Fig. 2. The support system was fabricated with a hinged support at one end and a roller support at the other. The supports were spaced at 2000 mm centre to centre. The size of the support system was adequate for resisting the ultimate applied load on the specimens. Fatigued slabs SF1, SF2, and SF3 were placed under cyclic loading with different cycle count, i.e., 1 million, 1.5 million and 2 million respectively. The different number of cycles employed in the fatigue tests was to represent the high-cycle fatigue range loading. The first phase investigated the behaviour of the slabs under static test up to failure (S1). The ultimate strength ( $P_{ult}$ ) of the slab obtained in this phase was used as a reference in determining the loading range of minimum ( $P_{min}$ ) and maximum ( $P_{max}$ ) for the fatigue test. The fatigue test loading point was kept the same as in static tests and the cyclic load was applied at constant fatigue stress level,  $S$  (Eq. (2)) at 0.6 as follows:

$$(S = f_{max}/f_r) \quad (2)$$

The slabs were tested according to sinusoidal waveform fatigue load between the minimum load applied at 20% of the ultimate strength,  $P_{ult}$  to keep the contact of the actuator with the RC slab and the maximum load at 65% of the ultimate strength.

### 2.3 Modal Testing

In this study, modal test was conducted to determine the dynamic characteristic of RC slabs by establish its modal properties at undamaged state (before fatigue test) and damaged state (after fatigue and static test). At each modal test was undergone, the actuator was removed when the dynamic characteristics of the RC slabs were extracted. The testing matrix is shown in Table 1. Modal parameters (frequencies, mode shapes, and damping ratios) of the slabs were extracted through Modal Testing

Table 1. Testing Matrix

Specimen designation	Loading type	Frequency rate (Hz)	Total number of load cycles ( $\times 10^6$ )	Time taken (hour)
S1	Static	-	-	-
SF1	Fatigue + static	2	1.0	138.89
SF2	Fatigue + static	2	1.5	208.33
SF3	Fatigue + static	2	2.0	277.78

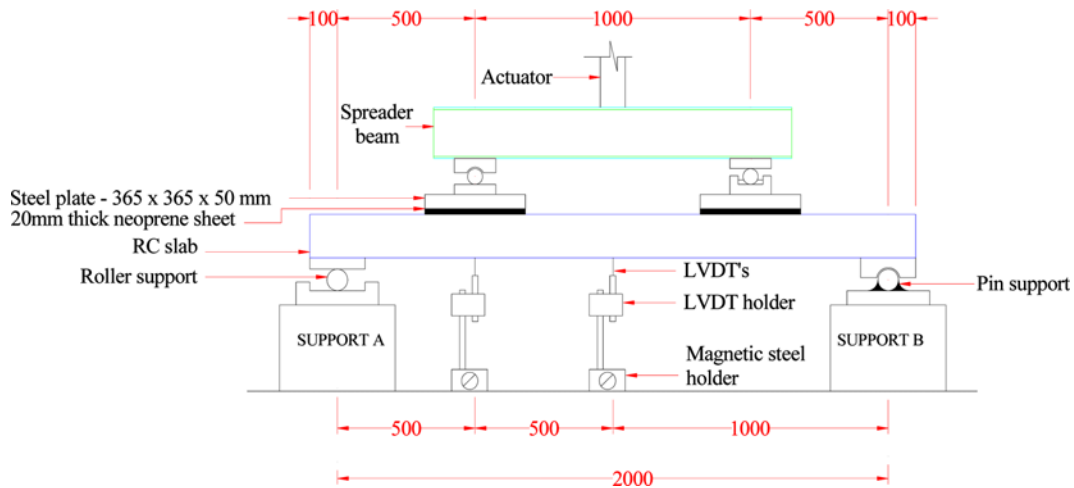


Fig. 2. Static and Fatigue Test Setup (unit in mm)

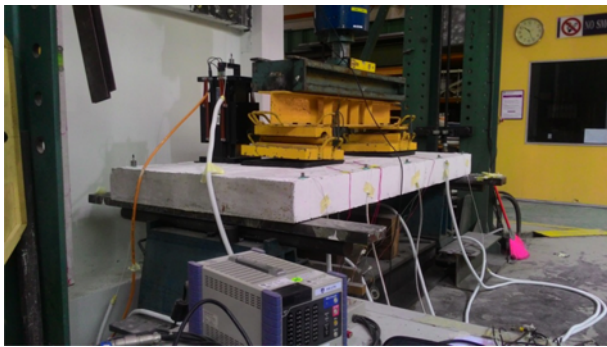


Fig. 3. Modal Testing Configuration

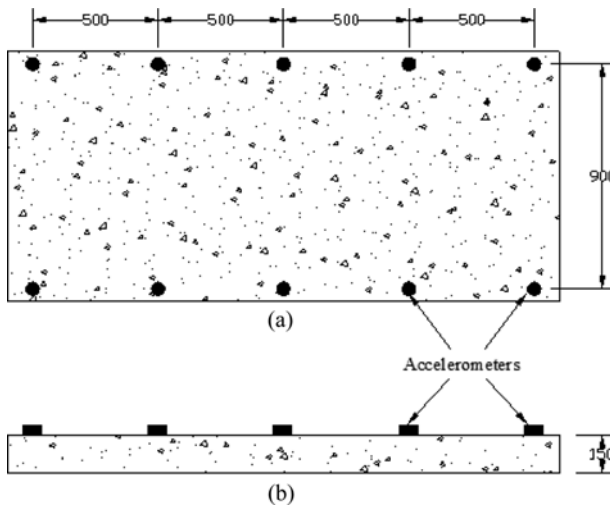


Fig. 4. Position of the Accelerometers and the Shaker on the Slab: (a) Plan, (b) Elevation (unit in mm)

(MT). The equipment used to perform the test where accelerometers, data acquisition system, and dynamic analyser as configured in Fig. 3. An electrodynamic shaker was used as an excitation source since the natural excitation level in the laboratory was too low as implemented by (Fernández *et al.*, 2011) for heavy and light structures. The output was directly

proportional to the current supplied by an amplifier. The force exerted on the slab was generated by the acceleration of a moving mass, which was attached to the shaker armature in the vertical direction. The structural responses were measured using ten accelerometers which were pre-mounted on the top surface of the slab along both its edges in the longitudinal direction at an equal spacing of 500 mm as illustrated in Fig. 4. All accelerometers were connected to a 24-channel dynamic analyser through connectors that supplied power and amplified the response signals.

### 3. Results and Discussion

#### 3.1 Modal Parameters from Experimental and Finite Element Model

Natural frequency, one of the modal parameters, is subjected to a certain degree of damage or deterioration by any change in stiffness which is shown in the relationship of simply supported beam as stated by Dahleh (2014) is expressed at Eq. (3):

$$\omega = (\beta_n L)^2 \sqrt{\frac{EI}{\rho L^4}} \quad (3)$$

where  $\omega$  is the natural frequency in rad/sec,  $(\beta_n L)^2$  is referring to the boundary conditions,  $n$  is the number of mode shape,  $E$  is the modulus of elasticity,  $I$  is the moment of inertia,  $\rho$  is the density, and  $L$  is the length of the beam. Fundamentally, as stiffness,  $EI$  is reduced in a structural system, the natural frequency also decreases and it can be concluded that the system has indeed undergone changes. Table 2 lists the numerical value of  $(\beta_n L)^2$  for typical end conditions corresponding to its number of modes. Subject to the theory, there are an infinite number of frequencies and mode shape, the structure has a fundamental natural frequency at the first frequency. At a higher frequency, the structure has a second frequency and mode shape, and a third, etc. The structure will also vibrate, deform, and take on different mode shapes depending on the mounting of the structure ends condition.

Table 2. Numerical Value of  $(\beta_n L)^2$  for Typical End Conditions (Dahleh, 2014)

	$(\beta_1 L)^2$	$(\beta_2 L)^2$	$(\beta_3 L)^2$
Beam configuration	Fundamental	Second mode	Third mode
Simply supported	9.87	39.5	88.9
Cantilever	3.52	22.0	61.7
Free-free	22.4	61.7	121.0
Clamped-clamped	22.4	61.7	121.0
Clamped-hinged	15.4	50.0	104.0
Hinged-free	0	15.4	50.0

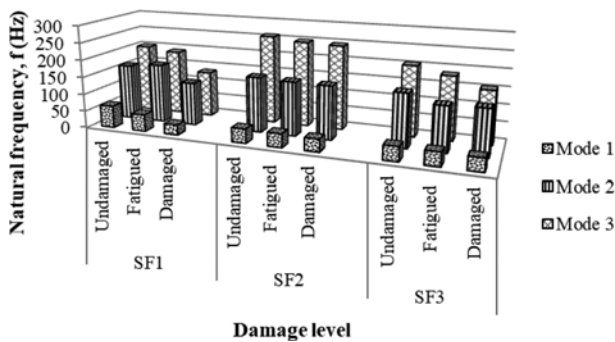


Fig. 5. Effect of Fatigued and Damaged Structures on Natural Frequency

Refer to Fig. 5, the results of the natural frequencies of all modes of the slabs are depicted by a bar graph against the damaged level. In principle, a certain degree of damage is mainly influencing the stiffness distribution. Consequently, it causes the natural frequency to change. The magnitude of the changes is also a sign of the severity of the damage. Although in visually there is no cracking line after cyclic load, however, the dynamic characteristics detect the internal deformation, this is apparent in the changes in natural frequency and damping ratio. In general, the trend for the natural frequencies decline was associated with the increasing of damage level subjected to the cyclic loads as shown in Fig. 5. A decrease in natural frequency was continuously observed at damaged RC slab after static load, it could be concluded that the structure experienced a greater loss of stiffness and later bigger decrease in natural frequencies. The magnitude of degradation may also become an indicator to the severity of damage induced onto the structure. The measured mode shapes that corresponding to these natural frequencies of undamaged, fatigued (SF1, SF2 and SF3) and damaged RC slabs are depicted in Figs. 6, 7 and 8, respectively.

The trend of the modal damping ratio of lower mode for the test fatigued RC slabs is shown in Fig. 9. These ratios represent the loss of energy from the system results in the decay amplitude the free vibration. The energy lost per cycle due to a damping force,  $F_d$  is computed from the general equation (Eq. (4)), in which  $W_d$  depends on several factors such as frequency or amplitude, as follows:

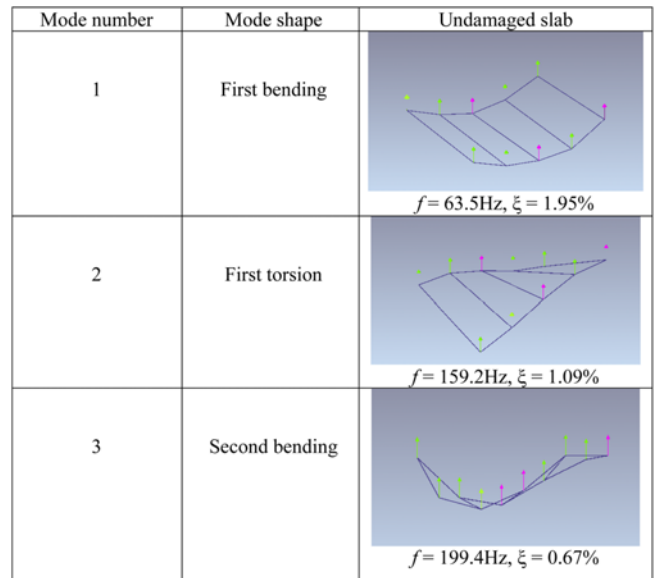


Fig. 6. Mode Shapes of Undamaged RC Slab, Identified as 1<sup>st</sup> and 2<sup>nd</sup> Bending (mode 1, mode 3) and 1<sup>st</sup>Torsion (mode 2)

$$W_d = \oint F_d dx \tag{4}$$

In general, the trend for the damping ratios obtained should increase as the level of fatigue gets worse. Apparently, the damping ratios obtained in this study are reflecting to the theory of damping factor.

For each of the natural frequency, it is corresponding to a natural state of vibration with a displacement configuration known as the normal mode or mode shape. In mathematical terms, it is related to the quantity and namely as Eigen vector. The mode shape has no unit. From the structure free vibration Eq. (5), and with a trial function of Eq. (6) then, the formula of Eigen equation is shown in Eq. (7). By solving this Eigen equation, Eigen vector,  $\{\phi\}$ , (mode shapes) and Eigen value,  $\omega^2$ , (natural frequency) will be acquired. In experimental work, the vibration of a structure was measured by accelerometers. By integrating its acceleration twice, the displacement,  $\{u(t)\}$ , can be obtained. The mode shape can be determined by transforming the acceleration using Fourier Transform.

$$[M]\{\ddot{v}(t) + [K]\{u(t)\}\} = \{0\} \tag{5}$$

$$\{u\} = \{\phi\} \sin \omega t \tag{6}$$

$$[K] - \omega^2 [M]\{\phi\} = 0 \tag{7}$$

The tested slabs have been modelled using commercial Finite Element (FE) modelling software to compare with the modal parameters obtained from the experimental. Initially, the model was developed by representing the undamaged slab by using the specific initial value of material properties. The concrete modulus of elasticity,  $E_{c,s}$  is 29,915 MPa, estimated using the empirical expression as calculated from Eq. (8) (Nawy, 2005) and the Poisson's ratio,  $\nu_c$  is 1.0.

$$E_{c,s} = 4730 \sqrt{f'_c} \tag{8}$$

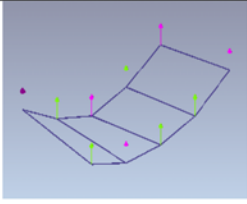
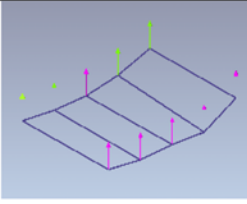
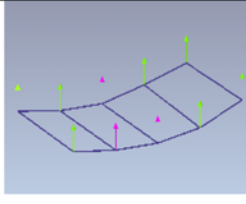
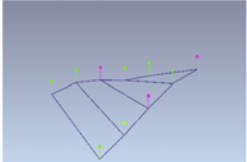
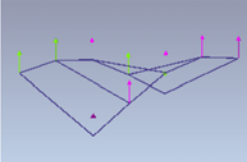
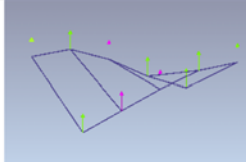
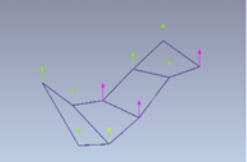
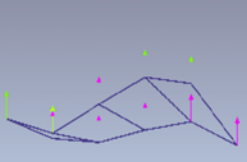
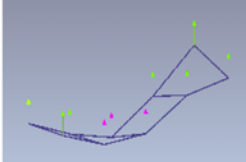
Mode number	Fatigue scenario		
	SF1	SF2	SF3
1	 $f = 48.2\text{Hz}, \xi = 1.36\%$	 $f = 41.0\text{Hz}, \xi = 1.6\%$	 $f = 39.0\text{Hz}, \xi = 2.43\%$
2	 $f = 170.0\text{Hz}, \xi = 1.44\%$	 $f = 153.0\text{Hz}, \xi = 0.97\%$	 $f = 128.7\text{Hz}, \xi = 1.84\%$
3	 $f = 189.0\text{Hz}, \xi = 1.21\%$	 $f = 203.6\text{Hz}, \xi = 0.44\%$	 $f = 183.0\text{Hz}, \xi = 2.45\%$

Fig. 7. Mode Shapes of Fatigued RC Slabs; SF1, SF2 and SF3, identified as 1<sup>st</sup> and 2<sup>nd</sup> Bending (mode 1, mode 3) and 1<sup>st</sup> Torsion (mode 2)

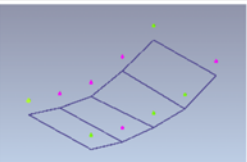
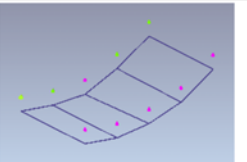
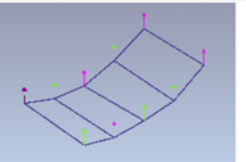
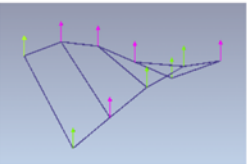
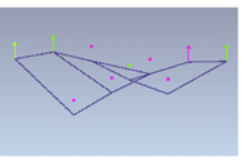
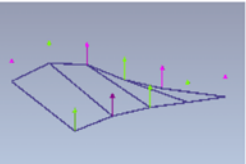
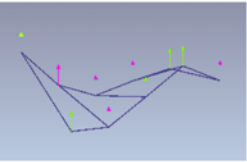
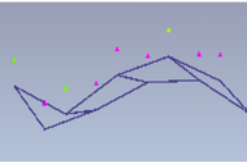
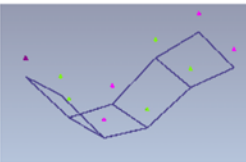
Mode number	Damage scenario		
	SF1	SF2	SF3
1	 $f = 38.6\text{Hz}, \xi = 1.57\%$	 $f = 36.0\text{Hz}, \xi = 2.27\%$	 $29.2\text{Hz}, \xi = 1.95\%$
2	 $f = 155.0\text{Hz}, \xi = 2.37\%$	 $f = 132.3\text{Hz}, \xi = 1.37\%$	 $f = 124.7\text{Hz}, \xi = 1.56\%$
3	 $f = 247.0\text{Hz}, \xi = 2.57\%$	 $f = 153.1\text{Hz}, \xi = 1.28\%$	 $f = 133.3\text{Hz}, \xi = 1.33\%$

Fig. 8. Mode Shapes of Damaged RC slabs; SF1, SF2 and SF3 Due to Static Load, identified as 1<sup>st</sup> and 2<sup>nd</sup> Bending (mode 1, mode 3) and 1<sup>st</sup> Torsion (mode 2)

For the geometry properties, the dimensions were taken as similar as in Fig. 1 to characterize the tested RC slabs. The numerical modelling computed the first three modes of natural frequencies for the initial FE model of RC slab structure which

correspond to the first bending, first torsion and second bending mode shapes, respectively, as depicted in Fig. 10. The degree of similarity of modal parameters can be examined qualitatively and quantitatively through the correlation analysis. The updating



Fig. 9. Damping Ratios of Fatigued RC Slabs at Lower Mode

Table 3. Natural Frequencies Correlation between Experimental ( $f_{exp}$ ) and Initial Numerical ( $f_{fem,int}$ ) of the Undamaged RC Slab

Mode	Experimental, $f_{exp}$ (Hz)	FEM, $f_{fem,int}$ (Hz)	Error $\Delta_f = (f_{exp} - f_{fem,int})/f_{exp}$ (%)
1	63.5	67.57	-6.41
2	159.0	194.36	-22.24
3	199.0	263.94	-32.63

done by using the simple Eq. (9). The relative error ( $\Delta_f$ ) of the numerical natural frequency ( $f_{fem}$ ) is calculated against the experimental measured ( $f_{exp}$ ) as follows:

$$\Delta_f = \frac{f_{fem} - f_{exp}}{f_{exp}} \quad (9)$$

procedure starts with the model matching step. Generally, the most common correlation method used by analysts to make a direct comparison is through specific natural frequencies matched between the numerical and experimental model. This is often

The comparison of experimental and numerical results at initial undamaged state is presented in Table 3. The reasons of deviation between both methods may probably due to the

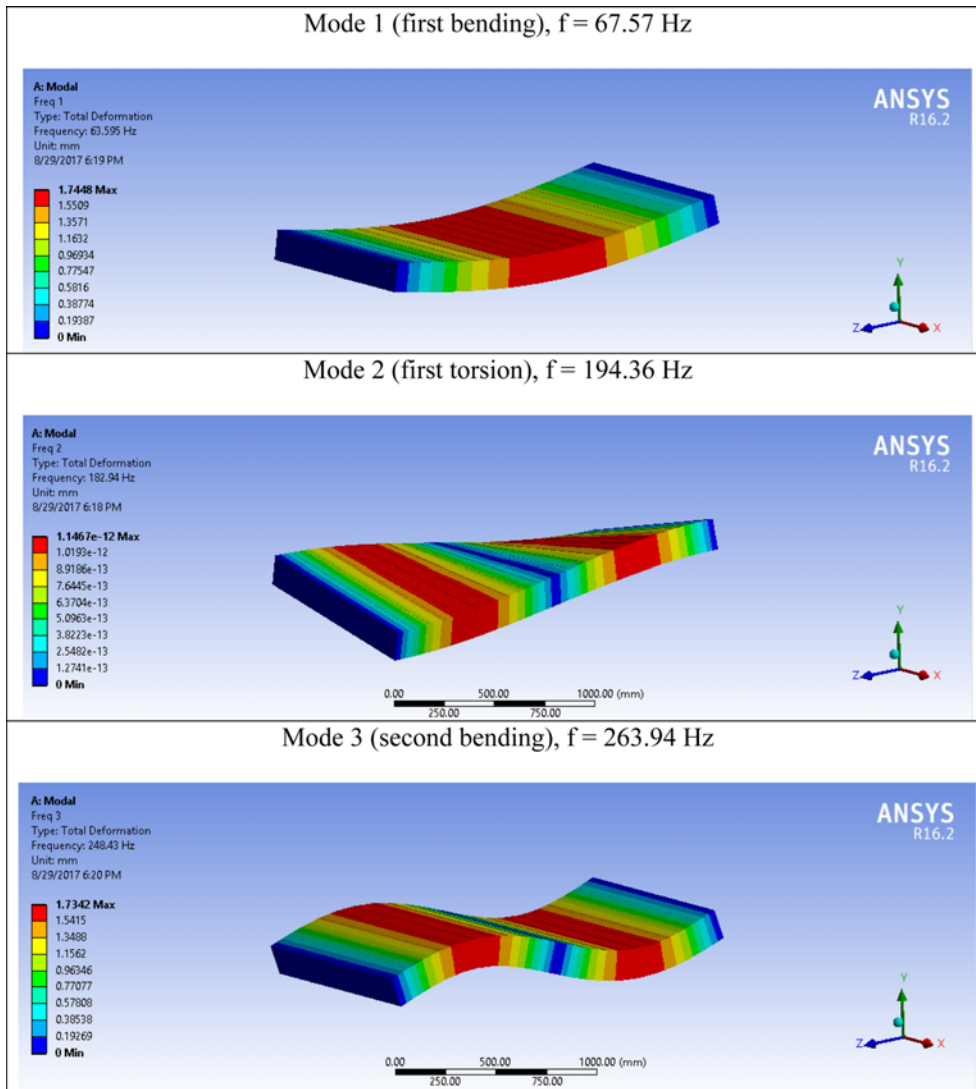


Fig. 10. The First Three Natural Frequencies and the Corresponding Mode Shapes of the Initial RC Slab FE Model, denominated as 1<sup>st</sup> Bending, 2<sup>nd</sup> Bending (mode 1, mode 3) and 1<sup>st</sup> Torsion (mode 2)

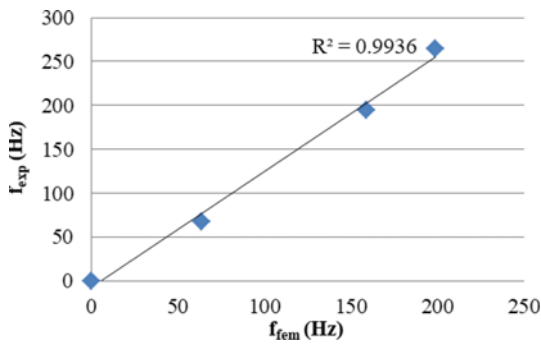


Fig. 11. Comparison between Initial Numerically Calculated ( $f_{fem}$ ) and Experimentally Estimated ( $f_{fem}$ ) Natural Frequencies

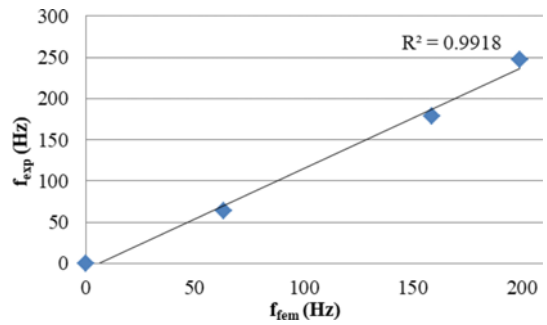


Fig. 12. Correlation of Updated Numerical ( $f_{fem}$ ) and Experimental Measured ( $f_{fem}$ ) Natural Frequencies of Undamaged RC Slab

Table 4. Natural Frequencies Correlation between Experimental ( $f_{exp}$ ) and Updated Numerical ( $f_{fem,updt}$ ) of the Undamaged RC Slab

Mode	Experimental, $f_{exp}$ (Hz)	FEM, $f_{fem,updt}$ (Hz)	Error $\Delta f = (f_{exp} - f_{fem,updt})/f_{exp}$ (%)
1	63.5	63.3	0.31
2	159	182.9	-12.01
3	199	248.4	-24.15

boundary condition, geometry and material features in simulation are not fully the same as that of the tested structures. Eq. (9) quantifies the difference of natural frequencies from experimental and numerical. A linear graph can also be used by plotting the experimental value against the numerical value for each of the modes. The good correlation of perfectly matched between the two sets of results was displayed as a straight line on the graph with the regression value of 0.9936 as shown in Fig. 11.

In order to match the experimental natural frequencies, the initial FE model needs to be updated by varying the material and geometry properties of the slab structure. The updating exercise was conducted using the same FE modelling software under parametric optimization. In the updating process, the selected uncertain parameters were constrained with upper and lower limit values based on engineering judgement to guarantee the physical significance that reflects the real structure. The comparison of experimental and updated numerical results at undamaged state is presented in Table 4. It shows that the first frequency differences reduced from 6.41% to 0.31% which explains the updated FE model has reflected the real dynamic behaviour of the structure. The other ways to correlate the difference is by showing some pairing of both results by indicating the regression linear values close to 1.0, as presented in Fig. 12. However, the error was high in the second mode as compared to the first and third mode, this is because modal data for torsion mode is not so precise in both numerical and experimental. The effects on higher modes may also be affected by the ambient effects on the modal test which can be contaminated by the noise signal. From correlation analysis, considering the updated FE models are good

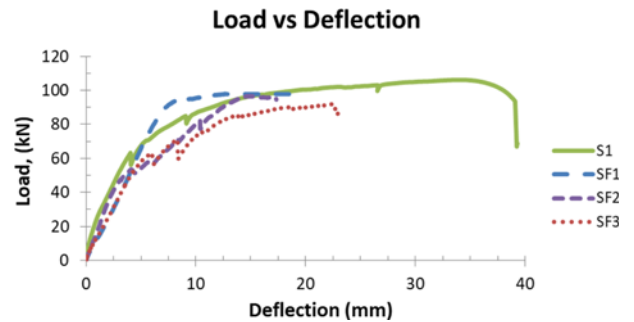


Fig. 13. Load-deflection Curves of Slabs SF1, SF2, and SF3 due to Static Load, Compared with Control Slab S1 that is not Preloaded with Fatigue Load

candidates to be used for the next prediction of the FE model for fatigued and damaged structures.

### 3.2 Mechanical Behaviour of Fatigued Slabs

As shown in Fig. 13, the load-deflection curves for the monotonic slab tests demonstrated a nearly tri-linear response. The first segment of the curves linearly varies which full elastic behaviour with negligible deflection up to the first cracking. It is characterized as pre cracking stage, where a structural member is crack-free. In this region the most loaded slab, SF3 accelerate the first cracking process of the fatigued slab as compared to the slab SF2 and SF3. The second region of the load-deflection behaviour extended from post cracking to yielding of the internal reinforcement of the slabs. In this region, most slabs lie at service loads. The progression of the flexural cracking contributes to the reducing of the section flexural rigidity and hence it was exhibited in the less steep of load-deflection curves compared to pre cracking stage segment. In this stage, reduced strength and stiffness were displayed in the most fatigued slab SF3 as compared to less fatigued slab of SF1 and SF3. The last third region of the load-deflection curve was the post serviceability stage, where the stress in the tension reinforcement reaches the limit state of the yielding and up to failure. The residual load capacity of slab SF1 was found to be 98.1 kN. The residual load capacities of slab SF2 was 96.7 kN, which is

1.4% lower than that of slab SF1 due to the higher number of load cycles applied to it. Slab SF3, which was put under the highest number of load cycles of 2 million, had the lowest residual load capacity of the slabs. The residual load capacity of SF3 was 92.1 kN, by which this value is 4.75% and 6.1% lower compared to slab SF2 and slab SF1 respectively. The results indicated that the strength of the fatigued RC slabs was decreased as fatigue level on the RC slabs increased, which is shown the structural stiffness reduced. This decreasing value of stiffness is due to the yield of steel tensile. It is also noticed that the residual load capacities of fatigued slabs are lower than unfatigued RC slab S1. It can be concluded that the residual load capacities of the fatigued slabs were influenced significantly by the accumulated fatigue damage, although it should be noted that all the slabs did not fail due to fatigue. The change in structural stiffness not only occurs in damaged slabs but also in fatigued slabs. During the cyclic loading, the concrete between the surrounding reinforcements is subjected to tensile fatigue. Thus, its modulus of rupture,  $f_r$  decreases with increasing number of cycles. The relation between the modulus of rupture at first cycle, and at a certain number of cycles  $N$ ,  $f_{r,N}$  can be expressed in Eq. (10) (ACI-318, 2008):

$$f_{r,N} = f_r \left( 1 - \frac{\log N}{10.954} \right) \quad (10)$$

Then, this equation is used to calculate the cracking moment,  $M_{cr,N}$  (Eq. (11)) which was decreases with the number of cycles, and consequently the average stiffness of the slab given by Eq. (12):

$$M_{cr,N} = \frac{I_g}{(h-y)} f_{r,N} \quad (11)$$

$$I_{E,N} = I_{cr,N} + \left( \frac{M_{cr,N}}{M_a} \right)^3 (I_g - I_{cr,N}) \quad (12)$$

The stiffness degradation in fatigue structures is because of the time-dependency on cyclic creep strain of concrete after  $N$  fatigue cycles, which is also influenced by the secant modulus of elasticity for concrete in compression,  $E_N$  as shown in Eq. (13):

$$E_N = \frac{\sigma_{max}}{\frac{\sigma_{max}}{E} + \epsilon_c} \quad (13)$$

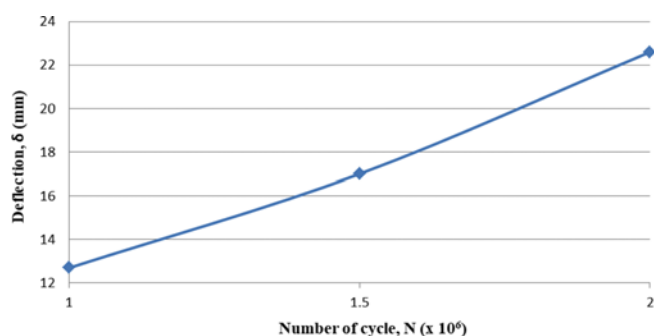


Fig. 14. Deflection of the Slab Appropriate to the Number of Cycles

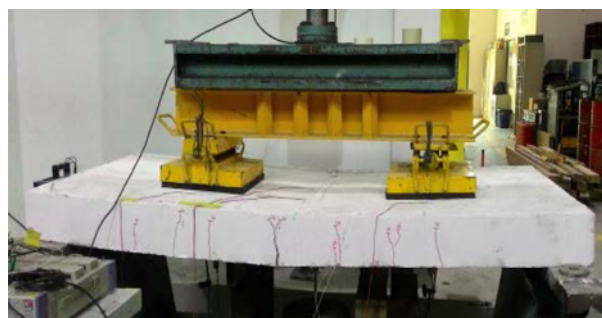


Fig. 15. Flexural Crack near the Load Actuator Position and Propagated towards the Support of the Slab

Figure 14 shows the change in deflection of the slabs as the number of cyclic load increases. It can be seen that the amount of slab deflection increases with the total cycles applied. The flexural crack was observed near the load actuator position and propagated toward the support of the slab, as shown in Fig. 15. The deflection behaviour of the slabs under cyclic loading shows a uniform increase in percentages of 34% and 33%, corresponding to 1.5 million and 2 million number of cyclic loads, respectively. Similar trends were also reported in the investigations carried out by Carvelli *et al.* (2010); Cheng (2011); Foglar and Göringer (2015); and Peng *et al.* (2016).

#### 4. Conclusions

Three reinforced concrete slabs were tested under a different number of cyclic loads and under static load up to ultimate. Modal tests were conducted after each step of loading to assess their dynamic performance by evaluating the modal parameters. The dynamic and mechanical properties of these fatigued RC slabs were investigated experimentally and numerically. The results have shown that the intensity of fatigued structures causes significant changes to the modal parameters and structural loading capacity. It has been found that the changes in natural frequencies are also consistent with the damage accumulation corresponding to cyclic loads and the residual load carrying capacity as obtained from static load tests. The changes in natural frequencies for different conditions of damage can be linearly represented by stiffness degradation. The relationship between the mechanical and dynamic behaviour of structures in term of residual load carrying capacity, number of cycles, and natural frequency have been established. A modelling based on finite element and updating has been presented to validate the dynamic characteristics obtained from experimental. Hence the modelling could be used for the prediction of the structures in the future. Thus, the findings have strengthened the viability of non-destructive techniques, in particular, modal testing for detection and quantification of damages whereby it is not limited to damage condition only but also extended in fatigue stage.



## Acknowledgements

This research was supported by Fundamental Research Grant Scheme (FRGS-FP004/2014B), Ministry of Education, Malaysia and University Malaya High Impact Research (HIR-UM.C/HIR/MOHE/ENG/36 (D000036-16001). Authors would like to thank all technicians in Heavy Structural Laboratory and Concrete Laboratory, Department of Civil Engineering, University Malaya and Faculty of Civil Engineering, University Technology MARA, Malaysia.

## References

- ACI-318 (2008). *Building code requirements for reinforced concrete*, American Concrete Institute, USA, pp. 122-124.
- Altunışık, A. C., Karahasan, O. Ş., Genç, A. F., Okur, F. Y., Günaydin, M., and Adanur, S. (2018). "Sensitivity-based model updating of building frames using modal test data." *KSCE Journal of Civil Engineering*, Vol. 2, No. 10, pp. 4038-4046, DOI: 10.1007/s12205-018-1601-6.
- Bayraktar, A., Can Altunışık, A., Sevim, B., and Türker, T. (2010). "Ambient vibration tests of a steel footbridge." *Journal of Nondestructive Evaluation*, Vol. 29, No. 1, pp. 14-24, DOI: 10.1007/s10921-009-0061-9.
- Benmokrane, B., El-Salakawy, E., El-Ragaby, A., and Lackey, T. (2006). "Designing and testing of concrete bridge decks reinforced with glass FRP bars." *Journal of Bridge Engineering*, Vol. 11, No. 2, pp. 217-229.
- BS 1881 (1983). *Part 120: Testing concrete. Method for determination of compressive strength of concrete cores*, British Standards Institution, London, pp. 1-5.
- BS 4449 (2005). *Steel for the reinforcement of concrete - weldable reinforcing steel - bar, coil and decoiled product - specification*, British Standards Institution, London, pp. 1-34.
- Carreira, M. R., Dias, A. A., and de Alcântara Segundinho, P. G. (2017). "Nondestructive evaluation of corymbia citriodora logs by means of the free transverse vibration test." *Journal of Nondestructive Evaluation*, Vol. 36, No. 2, pp. 1-7, DOI: 10.1007/s10921-017-0401-0.
- Carvelli, V., Pisani, M. A., and Poggi, C. (2010). "Fatigue behaviour of concrete bridge deck slabs reinforced with GFRP bars." *Composites Part B: Engineering*, Vol. 41, No. 7, pp. 560-567, DOI: 10.1016/j.compositesb.2010.06.006.
- Cheng, L. (2011). "Flexural fatigue analysis of a CFRP form reinforced concrete bridge deck." *Composite Structures*, Vol. 93, No. 11, pp. 2895-2902, DOI: 10.1016/j.compstruct.2011.05.014.
- Dahleh, W. T. T. and M. D. (2014). *Theory of Vibrations with Applications*, (5<sup>th</sup> Ed.). England: Pearson, USA, pp. 271-273.
- Fernández, P., Reynolds, P., and Aenlle, M. L. (2011). "Experimental evaluation of mass change approaches for scaling factors estimation." *Dynamics of Civil Structures*, Vol. 4, pp. 109-118.
- Foglar, M. and Göringer, J. (2015). "Influence of cyclic loading on the deflection development of concrete specimens." *Civil Engineering Journal*, Vol. 4, No. 24, pp. 1-22, DOI: 10.14311/CEJ.2015.04.0024.
- Hsu, T. T. C. (1981). "Fatigue of plain concrete." *ACI Journal Proceedings*, Vol. 78, No. 4, pp. 292-305, DOI: 10.14359/6927.
- Kashif Ur Rehman, S., Ibrahim, Z., Memon, S. A., and Jameel, M. (2016). "Nondestructive test methods for concrete bridges: A review." *Construction and Building Materials*, Vol. 107, pp. 58-86. DOI: 10.1016/j.conbuildmat.2015.12.011.
- Ko, J. M. and Ni, Y. Q. (2003). "Structural health monitoring and intelligent vibration control of cable-supported bridges: Research and application." *KSCE Journal of Civil Engineering*, Vol. 7, No. 6, pp. 701-716, DOI: 10.1007/BF02829139.
- Kourehli, S. S., Bagheri, A., Amiri, G. G., and Ghafory-Ashtiany, M. (2013). "Structural damage detection using incomplete modal data and incomplete static response." *KSCE Journal of Civil Engineering*, Vol. 17, No. 1, pp. 216-223, DOI: 10.1007/s12205-012-1864-2.
- Kutunis, M., Boru, E. O., and Işık, E. (2017). "Alternative instrumentation schemes for the structural identification of the reinforced concrete field test structure by ambient vibration measurements." *KSCE Journal of Civil Engineering*, Vol. 21, No. 5, pp. 1793-1801, DOI: 10.1007/s12205-016-0758-0.
- Lenschow, R. (1980). "Long term random dynamic loading of concrete structures." *Materials and Structures*, Vol. 13, No. 3, pp. 274-278, DOI: 10.1007/BF02473567.
- Liu, Y., Fan, H., He, J., and Wu, D. (2012). "Static and fatigue experimental study on flexural behavior of hybrid GFRP-concrete bridge decks." *The Third Asia-Pacific Conference on FRP in Structures*, Sapporo, Japan, pp. 7.
- Nawy, E. (2005). *Reinforced concrete: A fundamental approach*, (5<sup>th</sup> Ed.), Pearson, Prentice Hall, NJ, USA, pp. 266-274.
- Oh, H., Sim, J., and Meyer, C. (2005). "Fatigue life of damaged bridge deck panels strengthened with carbon fiber sheets." *ACI Structural Journal*, Vol. 102, No. 1, pp. 85-92, DOI: 10.1016/S1359-8368(03)00044-1.
- Peng, H., Zhang, J., Shang, S., Liu, Y., and Cai, C. S. (2016). "Experimental study of flexural fatigue performance of reinforced concrete beams strengthened with prestressed CFRP plates." *Engineering Structures*, Vol. 127, pp. 62-72. DOI: 10.1016/j.engstruct.2016.08.026.
- Plachy, T. and Polak, M. (2007). "Fatigue damage identification on concrete structures using modal analysis." *3<sup>rd</sup> WSEAS International Conference on Applied and Theoretical Mechanics*, Spain, pp. 14-16.
- Prasad, D. R. and Seshu, D. R. (2010). "Study on change in modal parameters of RC beams due to fatigue type damage." *Asian Journal of Civil Engineering*, Vol. 11, No. 4, pp. 521-532.
- Sivagamasundari, R. and Kumaran, G. (2008). "A comparative study on the flexural behaviour of one-way concrete slabs reinforced with GFRP reinforcements and conventional reinforcements when subjected to monotonic and repeated loading." *The Open Civil Engineering Journal*, Vol. 2, No. 1, pp. 24-34, DOI: 10.2174/1874149500802010024.
- Suthiwarapirak, P. and Matsumoto, T. (2006). "Fatigue analysis of RC slabs and repaired RC slabs based on crack bridging degradation concept." *Journal of Structural Engineering*, Vol. 132, pp. 939-949, DOI: 10.1061/(ASCE)0733-9445(2006)132:6(939).
- Yoon, M. K., Heider, D., Gillespie, J. W., Ratcliffe, C. P., and Crane, R. M. (2009). "Local damage detection with the global fitting method using mode shape data in notched beams." *Journal of Nondestructive Evaluation*, Vol. 28, No. 2, pp. 63-74, DOI: 10.1007/s10921-009-0048-6.